SFB880: FLIGHT DYNAMICS

P. Horst[d], D. Keller[a], J.H. Diekmann[b], I. Krukow[c], K. Sommerwerk[d]
[a] DLR Braunschweig, Inst. of Aerodynamics and Flow Technology, Lilienthalplatz , 38108 Braunschweig
[b] DLR Braunschweig, Inst. of Flight Systems, Lilienthalplatz 7, 38108 Braunschweig,
[c] TU Braunschweig, Inst. f. Statik, Beethovenstr. 51, 38106 Braunschweig
[d] TU BS, Inst. of Aircraft Design and Lightweight Structures, Hermann-Blenk-Str. 35, 38108 Braunschweig

Abstract

The paper summarizes approaches and first results on flight dynamics of the Collaborative Research Centre SFB 880 - "Fundamentals of High Lift for Future Commercial Aircraft" - , i.e. high fidelity solutions of dynamics in aerodynamics, aeroelasticity and flight control.

1. INTRODUCTION

The basis of the entire Collaborative Research Centre are heavily linked subjects, namely the active high lift by means of the Coanda effect used in the area of the flap, the question how noise can be minimized and related subjects [1].
From preliminary, overall design the configuration of the aircraft is clearly influenced by the ability of using active high lift devices on one hand and restrictions due to engine failure during take-off etc. on the other hand.

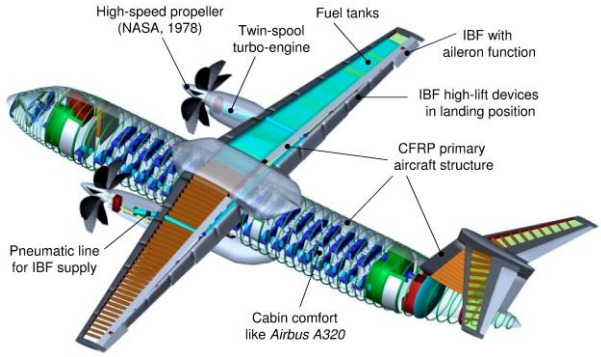

FIGURE 1: Reference aircraft configuration, from [1]

As visible in FIGURE 1, the reference configuration is a high wing configuration with a T-version of a VTP. It is also visible that the high lift flaps are extended to extreme deflections. The results presented here are using this reference plane for calculations, but the general output is not restricted to this individual configuration. As mentioned above, the active flow control uses the Coanda effect, where a thin jet accelerates the boundary layer near the slot in a way that the flow stays attached even at high deflections of the flap. In order to characterize this jet a moment coefficient c_μ is used. The moment coefficient cm is defined by the ratio of introduced jet momentum per time to the onflow dynamic pressure q_∞ and the wing reference area S_{ref}.

$$c_\mu = \frac{v_{jet}\dot{m}_{jet}}{qS_{ref}} \quad , \quad q = \frac{1}{2}\rho_\infty v_\infty^2$$

Dynamics obviously play a key role in aerodynamics, aeroelasticity and directly are needed for the simulation of the flight control. Therefore, these heavily linked subjects are treated together in this paper.

2. DYNAMICS OF LIFT GENERATION

2.1. Introduction

The aim of this sub-project of the Collaborative Research Centre is to examine numerically the effects circulation control has on the handling qualities of an aircraft and to derive possible constraints regarding aircraft design. The results also improve a database, which enables the aircraft maneuver simulation and the development of a flight control system (see chapter 3). Therefore, steady as well as unsteady Reynolds-Averaged-Navier-Stokes (RANS) simulations were performed. The work started with basic investigations. After performing mesh topology and grid convergence studies [6] in order to establish a best practice for the mesh generation for this kind of configuration, the fundamental behavior and interaction of a wing and horizontal tail plane were investigated in 2D with representative sections of the main wing and the horizontal tail plane (HTP) of the reference aircraft. In addition to the assessment of the longitudinal static stability, unsteady calculations were performed to gain an idea of the dynamic behavior. This includes the estimation of dynamic derivatives as well as the start-up behavior when activating or deactivating the circulation control [3]. The extension of the work to 3D again began with a meshing study, which investigated wake resolution requirements and was followed by a basic investigation of the aircraft specific circulation control blowing parameters [6]. Afterwards, the longitudinal static stability and controllability of the reference aircraft with and without engine effects were evaluated [4]. Furthermore, critical failure cases, namely the one engine inoperative (OEI) case as well as an asymmetric circulation control failure were assessed [4]. The following sections focus on the fundamental results of the 3D simulations by discussing

the static behavior of the landing configuration, the impact of installed turboprop engines and the aircraft behavior for selected failure cases.

2.2. Computational Results

2.2.1. Fundamental Aerodynamic Behavior

The investigation of the 3D model began with a basic analysis of the aerodynamic behavior for the tail-off configuration when circulation control is applied. Therefore, several blowing coefficients where investigated, which characterize the individual correlation between the lift coefficient and the jet momentum coefficient. At a jet momentum coefficient of c_μ=0.033, the configuration without engine is at the threshold between boundary layer control and super circulation and delivers a maximum lift coefficient of c_L = 3.46 (see FIGURE 2).

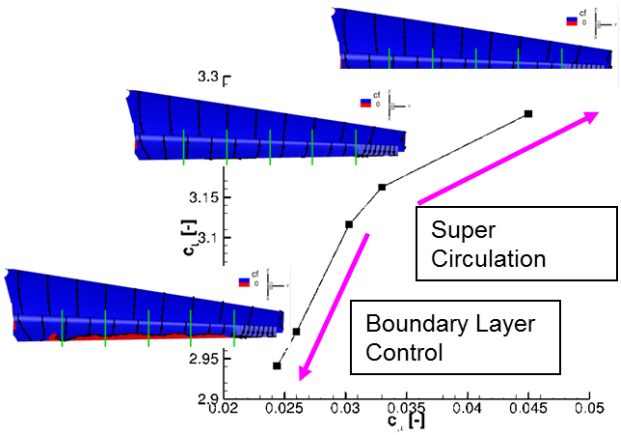

FIGURE 2: Correlation between flap separation and lift coefficient and jet momentum coefficient c_μ at α=0.0°

When thrust is applied, the lift is further increased to c_L=4.09 at $c_{t,T2}$=0.42, whereas the maximum angle of attack is reduced. The additional lift can be primarily attributed to the locally increased dynamic pressure in the slipstream of the propeller (FIGURE 3). In consequence, the pressure on the lower surface of the main wing is increased, whereas the pressure on the upper surface is mostly reduced (FIGURE 4). However, the alteration of the leading edge suction peak is dependent on the location relative to the nacelle. While it is amplified on the upwash side of the propeller, it is reduced on the downwash side.

Due to the large flap deflection, the altered flow around the wing also has a significant impact on the drag coefficient, as the slipstream-flap impingement (FIGURE 5) leads to high pressure values on the lower side of the flap. As a result, the lift to drag ratio is reduced from $L/D_{c\mu=0.033,nT}$=6.7 to $L/D_{c\mu=0.033,Tmax}$=4.6.

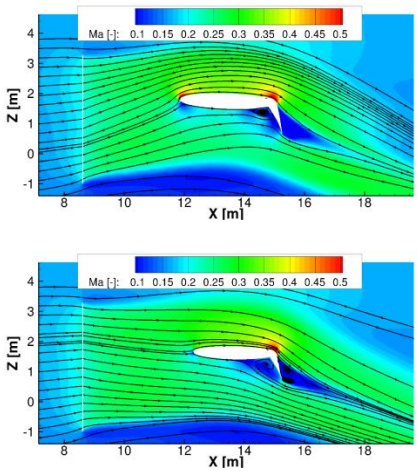

FIGURE 3: Flowfield around the main wing. Top: Propeller upwash region. Bottom: Propeller downwash region

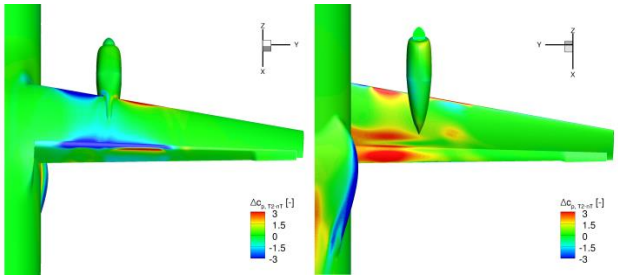

FIGURE 4: Delta c_p contour between maximum thrust and zero thrust

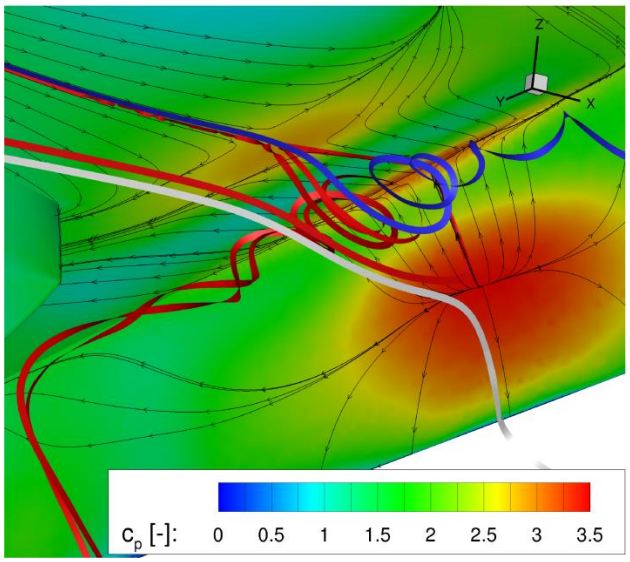

FIGURE 5: Slipstream-flap impingement inboard of the nacelle

2.2.2. Static Longitudinal Motion

For the evaluation of the flight dynamical behavior of an aircraft, the longitudinal static stability and controllability are two fundamental characteristics. While the controllability demonstrates the capability to trim an aircraft at a certain position of center of gravity (c.g.), the

longitudinal static stability is an indicator of the behavior of an aircraft after a disturbance in the angle of attack. The investigation of the longitudinal stability and controllability for the landing configuration was performed at an angle of attack of α=0°.

The controllable range of the center of gravity (c.g.) position is impacted by circulation control and slipstream effects in several ways. First, increased blowing and engine thrust lead to an enhanced lift generation of the main wing, which consequently results in a higher pitching moment. Eventually, the range of controllable c.g. positions is reduced. Furthermore, the increased circulation of the main wing causes a stronger downwash at the horizontal tail plane (HTP), which would lead to a shift of the c.g. range towards the front if the possible tail plane deflection is restricted to a certain range. However, if thrust is applied, the propeller itself delivers an additional pitching moment, which moves the c.g. range towards the front due to the high wing mounted engine. In case of high thrust coefficients, the shift can be significant.

A variation of the jet momentum coefficient and the thrust coefficient also impacts the HTP trim angle, whereas the magnitude depends on the c.g. location. For the selected c.g. position, which reflects the mass distribution at maximum landing weight and maximum payload, the difference in the HTP trim angle is rather small. From c_μ=0.024 to c_μ=0.033, the HTP trim angle is increased by $\Delta\, i_{HTP}$=0.4°. Here, the higher nose down pitching moment of the main wing is counteracted by an increased pitch up moment of the HTP due to the strengthened downwash. When thrust is applied, the main wing's pitching moment is further increased and therefore amplified by the additional positive pitching moment of the HTP due to the increased downwash. However, the negative pitching moment of the propeller limits the difference of the trim angle to $\Delta\, i_{HTP}$=2.2°.

The investigation of the longitudinal static stability showed that the thrust negatively influences the stability limit. The pitching moment gradient of the main wing is increased due to an additional load in the inboard region. In addition, the propeller delivers a positive pitching moment gradient and the negative slope of the HTP's pitching moment curve is flattened. As a result, the stability limit moves towards the nose.

2.2.3. Failure Cases

Due to the relatively large propeller diameter, the failure case *one engine inoperative* (OEI) is particularly important for the vertical tail plane (VTP) design. Regarding the aileron design, an asymmetric failure of the circulation control is thought to be the critical case. Therefore, both an OEI case as well as an one-sided circulation control failure were simulated. As expected, the former leads to a high yawing moment whereas the latter causes strong rolling moments. However, the magnitude of the resulting yawing moments is unexpectedly high. In case of OEI, the yawing moment caused by the asymmetric thrust more than doubles due to a contribution from the fuselage and the vertical tail plane (VTP). The lateral forces on the fuselage and the VTP arise from a helical flow around the fuselage, which is associated with the asymmetric lift distribution (FIGURE 6).

2.3. Outlook

To date, the investigation of the 3D model was limited to the static behavior. In future, unsteady RANS calculations are planned to determine the dynamic derivatives of the longitudinal motion. Furthermore, the lateral motion will be further investigated. It is expected that the propeller slipstream has a significant influence on the directional stability.

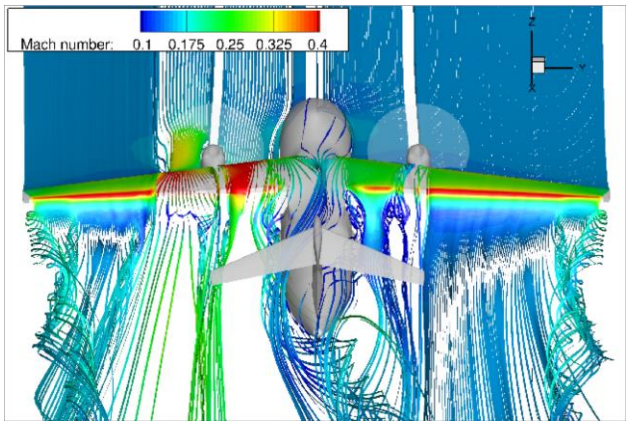

FIGURE 6: Wake evolution at maximum thrust and one engine inoperative

3. CONTROL CONCEPTS

3.1. Main Target

The focus of this project is to analyze the flight mechanics of an active high lift aircraft in order to make sure that this aircraft can be operated under highest safety standards and to use the opportunities of the system in order to extend aircraft control especially at low airspeed. Investigations will reveal the qualities of the aircraft in terms of stability and the possible demand for control. The special flight mechanical characteristics of an active high lift aircraft will also be investigated considering the feasibility to perform standard procedures for take-off and landing as well as new procedures e.g. for noise reduction which might take advantage of the special characteristics. It is likely that all these procedures need to be operated or can be improved by control systems.

The design of innovative control concepts by using the opportunities of an active high lift system is only possible with a proper understanding of the underlying flight dynamics of active high lift aircraft. The first step within this work is to create a nonlinear mathematical model, which describes the dynamic behavior of an active high lift aircraft and which provides direct access to the active high lift system in order to use it for aircraft control. The central focus lies on the development of a suitable model structure and the design of an aerodynamic derivative model. In addition an engine model which allows for usage of bleed air for blown flaps has to be established and integrated into the simulation environment.

The consistent further development of an existing model structure for conventional aircraft, as well as the identification of the aerodynamic model by analysis of SFB 880 created CFD results was the first target to achieve. The effects of the active high lift system on aerodynamics and the existing nonlinearities which are occurring due to stall are needed to be modeled. These nonlinearities also had to be reflected in the model for downwash and pitching moment. Further steps now will be the investigation of the resulting characteristics of the aerodynamic model and their impact on the longitudinal motion of the aircraft as well as the extension of the model in terms of lateral motion.

3.2. Basic Tools

The simulations are performed by using MATLAB/Simulink[1], which allows a combination of script based and block diagram modeling. As a source for general aircraft data the reference aircraft data generated by PrADO are used [5]. This database provides information about geometry, weight, inertia and engine characteristics of the aircraft. The aerodynamic coefficients are identified from CFD results provided by SFB partner projects [6].

The initial point to start modeling from is a basic aircraft model, which describes the dynamics of a conventional turboprop engine powered aircraft [7]. This model includes structures for various subsystems and offers the chance to start from a reliable working and already running model. From this point it is possible to create a new model by adaptation and extension of the existing structures and well known mathematical sub-models. Basic input values like aircraft geometry, weight and balance information and moments of inertia created by PrADO have to be adapted as well. The remarkable changes to be made are the development of an engine model which allows for the extraction of bleed air and the redesign of the aerodynamic model, which needs to be able to calculate the aerodynamic forces and moments considering the influences of the active high lift system and builds the core of the flight mechanical model.

Active high lift is defined by using pressurized blowing air or sucking air to increase the lift of an airfoil. The basic function of such a specific blown Coandă flap system is to preserve the lift increasing effect of the flap even for extremely high flap deflections [8,9]. The efficiency of the active high lift system can be divided into two sections, depending on the jet momentum of the blowing system. In the Boundary Layer Control (BLC) section the injected mass flow influences the boundary layer at the flap, whereas in the Circulation Control (CC) section a new circulation is induced by the strong jetstream of the blowing system. The BLC section has its minimum value defined by the point of flow separation from the flap. It is chosen to be the preferable section to operate in, due to its higher efficiency in the air mass flow to additional lift generation ratio. Nonetheless CC section will be investigated as well.

The model is based on CFD results which clearly indicate the characteristic of two different gradients for the two sections. A reference value $C_{\mu.Ref}$ has been defined which indicates the maximum value of the BLC section and the minimum value for the circulation control section. Below the minimum value $C_{\mu.min}$ the flow along the flap can be considered to be separated.

For CFD calculations DLR's Tau code [10] and the commercial tool VSAero[2] have been used. Aerodynamic data for wing/fuselage in clean configuration and horizontal tailplane have been created by the low fidelity CFD tool VSAero whereas the complex aerodynamics of the wing/fuselage in full flaps configuration with active high lift system have been calculated with the high fidelity Tau code. The operational limits in clean configuration as well as for the horizontal tail are approximated based on the VSAero results in terms of minimum/maximum values for angle of attack. The influence of the active high lift system on drag and pitching moment as well as on downwash can be separated into the same sections. Similar to lift, gradients along the jet momentum coefficient for the drag, pitching moment and downwash have been identified from CFD results.

3.3. Initial Developments

The aerodynamic model needs to reflect the influence of the active high lift system. A relation to the main parameter C_μ has to be established, which keeps aerodynamic forces and moments variable for different jet momentum values. The basic design of the aerodynamic derivative model is similar to classic designs used in flight dynamics models [11,12]. This model had to be extended in order to describe the lift increase due to the active high lift system. A two point model approach is used for modeling the generated aerodynamic lift and pitching moment. It separates the wing fuselage configuration from the horizontal tailplane. The main effect of the active high lift system influences the wing fuselage directly and the horizontal tail indirectly by the impact on the downwash angle. Its influence can be split into two sections with a different efficiency in increasing or decreasing forces and moments. FIGURE 7 shows the results for the lift slope model of the wing fuselage. The red line shows the reference value of the jet momentum. The jet momentum now can be varied in between the given boundaries (red and blue line).

Besides its influence on the lift of the WFC, the active high lift system has a severe impact on the resulting downwash of the wing, which hits the tail of the aircraft. The model for the resulting downwash angle ε describes this dependency as a function of the lift produced by the WFC and the effect of the active high lift system.

The approach of using an aerodynamic two point model allows a very realistic representation of the pitching moment. This way the resulting model can be composed of the pitching moment of the WFC, the additional pitching moment of the active high lift system and the resulting pitching moment from the horizontal tail which includes the influences of the strong downwash on the local angle of attack of the horizontal tailplane. The whole model can be followed up in [13].

[1] By MathWorks

[2] by Analytical Methods Inc.

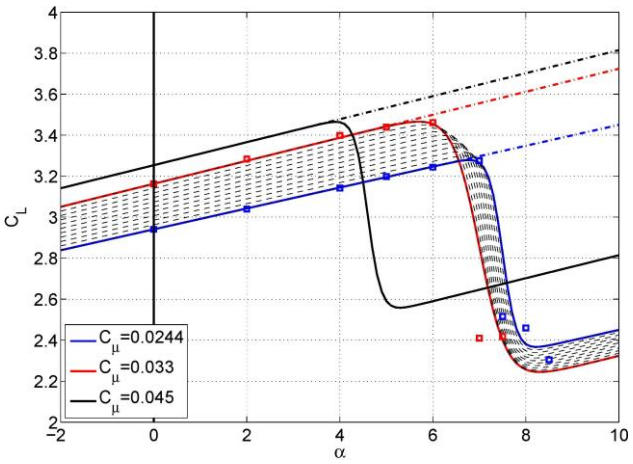

FIGURE 7: Lift for different jet momentum coeff.

3.4. Research Results

Recent research results from trim analysis indicate several flight mechanical occurrences due to the usage of an active high lift system. One of the major effects of active high lift system is the attainment of high lift coefficient values. These values are reached already at small maximum angles of attack. This leads to difficulties in pitch attitude for an approach situation, if the safety margins for approach speeds are taken into consideration. Another difficulty occurring is the high demand for nose up pitching moment by the horizontal tail to counteract the strong nose down pitching moment of the wing with the active high lift system. This moment is a result of the great suction peak at the trailing edge of the wing induced by the blown Coandă flap. Even though the described large negative downwash angles cause small trim incidence angles for the horizontal tailplane, the necessary local angle of attack at the horizontal tail to counteract the wings pitching moment has large negative values. This increases the risk of tail stall.

A possible solution to increase the maximum angle of attack of the wing fuselage configuration could be the integration of a leading edge device. Therefore respective research is carried out within the SFB 880 and will be evaluated after application to the simulation model. Additionally the local angle of attack of the horizontal tail can be reduced by replacing the symmetrical profile of the current horizontal tailplane by a profile with negative camber.
The center of gravity location also plays an important role for the controllability of the aircraft and thus the loading of the horizontal tail. These results show the influence of the active high lift system on flight mechanics which need to be considered e.g. in aircraft configuration design.

3.5. Outlook

The development of a flight mechanical model for an aircraft with active high lift system now opens a vast range of possibilities to investigate. Beside the currently performed trim, center of gravity, longitudinal control and static stability analysis, next steps will be dynamic behavior and procedure investigations. Additionally the lateral motion modeling is yet to come and will provide the opportunity to give answers to inevitable questions concerning safety during system failures and emergency situations. This way the subproject “control concepts” yields important contributions to the comprehensive active high lift research which SFB 880 seeks to provide to scientific community.

4. STRUCTURAL DESIGN AND AEROELASTICS

Aeroelastics obviously depend on a reliable structural design and need high fidelity analyses on one hand, but also reduced-order models for flight control applications. Both ways are treated in this chapter.

4.1. High Fidelity Model Generation, sizing and aeroelastic analyses

4.1.1. Objective

The aim of the first part of this subproject is on the one hand the structural sizing of the wing and the analysis of integration concepts for the blown flap duct system. On the other hand the quantifications of the effects of the elastic wing structures and their interaction with the airflow are analyzed. The local effects of the duct system slot and the global wing deflection are also considered. Since the aeroelastic effects of the wing can have a big influence on the overall aerodynamic performance.

An aircraft with blown flap circulation control has distinct differences in the loads during approach due to the induced Coandă effect. The flap systems are deployed to angles of up to 85° which not only results in larger pressure loads on the flaps but also considerably higher pitching moments. Analyzing the influence of these factors on the sizing of a detailed model of the wing is therefore of high importance.

In addition, the understanding of the aeroelastic phenomena of a wing with active circulation control is an important aspect for the overall aerodynamic performance of the aircraft. The stability of the boundary layer flow is critical to the circulation control. The deflection of the wing on the global scale as well as the deformation of the duct and flap structures will influence the flow in reality. High fidelity models are used for the computations of the structural deformations and its influence on the aerodynamics. This high fidelity approach is employed over the whole analysis process from the sizing of the structures to the aeroelastic analysis both on the global and local scale. This approach allows capturing even the finest effects of small deformations while the aerodynamics are modeled as close to reality as manageable with today’s resources.

4.1.2. Models and Methods

The analysis process uses two models on the structural side to capture the global and local effects. All models are derived from a database generated by the preliminary aircraft design tool *PrADO* [5]. This database allows the exact reproduction of high fidelity wing models and derived models for local analyses.

The first model is the complete wing with a half-span of 14.38 m and a quarter chord sweep of 7°. The taper ratio is 0.38 and the dihedral angle -2°. The aerodynamic reference of one wing is 47.5 m². The wing has six plain flaps, which account for 25 % of the chord. They are deflected to 65° for approach and landing while the

outboard flap operates as an aileron is deflected to 45°.

The second model is derived from the wing structure. It represents an untapered and unswept wing section with a width of one flap of 2.124 m and a chord length of 3.428 m being the mean aerodynamic chord (MAC) of the wing. The duct systems are represented in different configurations. The systems are integrated into the spoiler structure, the flap structure and directly into the wing box. The slot height of the blown air jet is set to 0.061 % of the chord which is 2.1 mm. The large difference in magnitudes is the driving factor for the high fidelity approach on the fluid and structural models.

The models are also detailed with stiffener elements like stringers. A composite material model is employed in both structural models. They are sized using a fully stressed design approach for global layer failure in addition to an analytical buckling estimation. The parameterized modeling is performed with *Patran*® while *ANSYS*® *Mechanical* is used as the structural solver. The sizing is terminated via a total mass change criterion. The employed load cases for sizing are approach and landing with deflected flaps as well as maneuver flight, gusts and cruise in clean configurations. All load cases are computed with high and low tank levels to account for the fuel loads [14].

The aerodynamic models are generated to solve the Reynolds-Averaged-Navier-Stokes equations (RANS) with the *TAU* code solver of the *German Aerospace Center (DLR)* [10]. The boundary layer interaction of the blown air jet with the oncoming flow is captured by high resolution grids. The grids are adapted for the global and local models. The global fluid meshes are generated with *Centaur* and *ICEM CFD* while the grids for flap section coupling are derived from 2D grids that are extruded in spanwise direction to achieve the desired resolution. The number of points is in the order of 25 million for the meshes used with active circulation control. All meshes are deformed according to the structural deformations during the coupling process.

The fluid structure interaction process uses a partitioned approach. The computed aerodynamic forces are conservatively transferred to the structures with the *ifls* coupling environment [15]. After solving the structural models with the imposed loads the resulting displacements are transferred back to the fluid meshes. Then the fluid meshes are deformed using a radial basis function approach.

The sizing of the structures uses a reduced one-step coupling process without the influence of the deformed structures on the aerodynamics for performance reasons.

4.1.3. Results

4.1.3.1. Sizing

The wing sizing took 17 iterations to complete and results in a weight of 3454 kg (c.f. FIGURE 8). The preliminary sizing with *PrADO* resulted in 3532 kg which is a difference of 2.2 % [4]. The high fidelity model is used in other projects in the SFB and allows working with a detailed mass distribution for flight dynamics. Exemplary wing displacements in z-direction are displayed in FIGURE 9 for the load cases 2.5g-maneuver and landing at specific iteration steps. The 2.5g maneuver results in the upward deflection. The landing load case results in downward deflection. grey: initial geoemtry, (a) iteration 2, (b) iteration 6, (c) iteration 17. The scale reflects the maximum displacements during the first iteration.

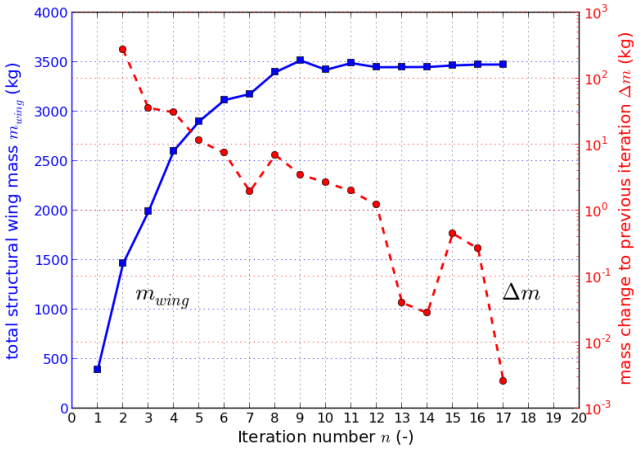

FIGURE 8: Global wing sizing convergence

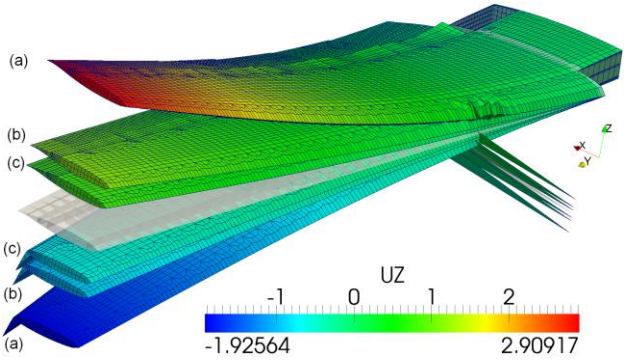

FIGURE 9: Exemplary wing displacement in z-direction.

The duct integration analyses result in a mass variation due to the different support structures employed. The overall mass of the flap section of external configuration is the highest. By integrating the duct into the flap or the spoiler the mass can be reduced by 3 % and 4 % respectively. This effect is due to the missing support structures which are needed for the external configuration [16].

4.1.3.2. Aeroelasticity

The local effects on the aerodynamics due to the deflection of the slot lip need to be considered. Since the structural dimensions near the slot are limited, stiffener elements are employed to keep the slot fixed. A variation in stiffener distance results in different deflections for the duct integration configurations. A limit of 10 % of the slot height is considered acceptable [14]. The flap integration always meets this limit while the external and spoiler integrations meet the limit at a stiffener distance of 125 and 110 mm [16]. The influence on the aerodynamics is still noticeable but is limited to a range of about 2 %. Some stabilization effects can also be recognized near the stall point for different c_μ values [17]. The external

configuration is favorable despite the weight disadvantage because of the ease of integration.

The effect of the global wing elasticity on the aerodynamic performance is analyzed. FIGURE 10 illustrates the small change in local lift coefficient over the wing span for different c_μ. Due to the high stiffness and the low sweep of the wing the influence is small and can be considered negligible. Only a small influence on the stall point appears for high jet momentums but can also be considered insignificant [17].

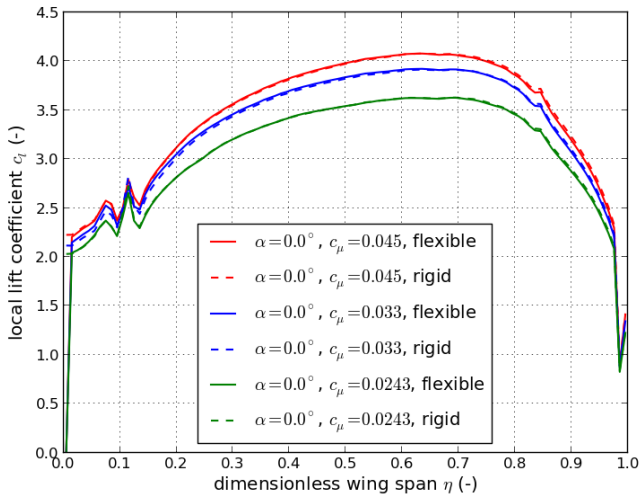

FIGURE 10: Global wing aeroelasticity effect

4.1.4. Outlook

In addition to the presented static aeroelastic effects the dynamic effects of local slot deformation and global low speed wing flutter are under consideration. Further work will include aero-structural optimizations of the wing structure by using Isogeometric Analysis (IGA) coupled with high-fidelity CFD.

4.1.5. Acknowledgement

The contributions of 3D grids by M. Burnazzi and D. Keller are gratefully acknowledged. The computations were made possible by access to the resources of the North-German Supercomputing Alliance (Norddeutscher Verbund zur Förderung des Hoch- und Höchstleistungsrechnens - HLRN).

4.2. REDUCED-ORDER MODEL

For extensive parameter studies investigating the aero-elastic behaviour of the airfoil, a reduced-order model is developed, which allows for simulations of different flight configurations with relatively low effort. It is tested for the most important aeroelastic instabilities, and the interesting case of bending flutter of a single degree of freedom including circulation control is shown, which has been described by Haas and Chopra [18]. Finally, a framework is developed to connect the reduced-order model of the elastic wing to the flight dynamics model of subproject on Flight Control (see chapter 3).

4.2.1. Structure and aerodynamics

In the preceding chapter, the airfoil structure is designed. A modal analysis performed in *ANSYS* gives back the natural frequencies ω_i and the natural modes $\hat{\mathbf{x}}_\mathbf{i}$, which are used for the reduction.

The aerodynamic behaviour is investigated at the two-dimensional profile section and mapped onto the three-dimensional airfoil using the strip theory. Numerical simulations of the flow around the profile are performed using the TAU-Code [19] of the German Aerospace Center (DLR) for a broad range of configurations. The varied parameters are the angle of attack α, the flap deflection angle δ_{fl} and the blowing coefficient c_μ. FIGURE 11 shows the lift coefficient from steady-state flow simulations at a flap deflection of 65°.

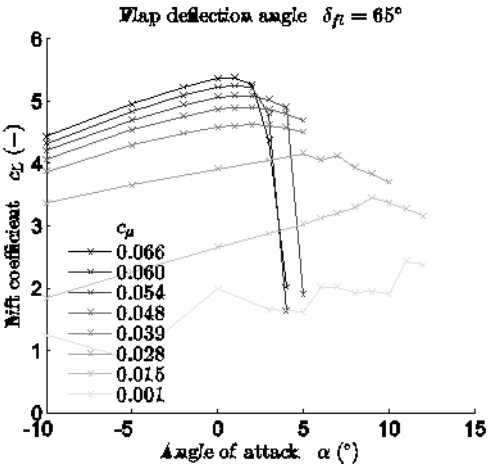

FIGURE 11: c_L as a function of c_μ and α

With this flap deflection, the flow can only be kept attached to the flap by making use of the Coandă stream. The higher the blowing coefficient c_μ, the higher is also the lift. Yet the angle of attack at which the highest lift is achieved is reduced to a few degrees.

For a mathematical description of the aerodynamic coef-ficients for lift and pitching moment, the numerical results are approximated by an optimised 4th order polynomial depending on α, δ_{fl}, and c_μ .Similarly, simulations of harmonic pitching oscillations are performed, from which the aerodynamic damping coefficients are derived.

4.2.2. Modal Reduction

The general form of the equation of motion is given by

$$(1)\quad \mathbf{M}\ddot{\mathbf{x}} + \mathbf{K}\mathbf{x} = \mathbf{L}(\mathbf{x}, \dot{\mathbf{x}}),$$

where the left-hand side describes the dynamics of the airfoil structure, and the vector **L** on the right-hand side contains the aerodynamic loads. Choosing the natural modes of the structure as a reduction basis, the structural and aerodynamic terms may be reduced separately and coupled in the modal space. Applying the modal ansatz

(2) $\mathbf{x} = \mathbf{X}\mathbf{q}$,

the equation of motion for a single generalised coordinate becomes

(3) $\ddot{q}_i + \omega_i^2 q_i = \hat{\mathbf{x}}_i^T \mathbf{L}(\mathbf{x}, \dot{\mathbf{x}})$.

On the right-hand side, the natural mode $\hat{\mathbf{x}}_i$ is given in the finite element discretisation of the structure, whereas the aerodynamic loads **L** are formulated in relation to the rigid body profile motions h and α using the strip theory. In order to match these, the modal matrix is transformed into the discretisation used for the description of the aerodynamic loads, which may be expressed formally by

(4) $\mathbf{X_A} = \mathbf{C}\,\mathbf{X}$.

Thus, the aerodynamic loads can be linked to the natural modes of the structure. As the aerodynamic loads are described by a polynomial, each of its terms can be reduced separately, so that the parameter dependencies are maintained in the reduced-order model. Hence, any flight configuration may be examined with the reduced-order model, without the need to back to the full-scale models.

4.2.3. Results

4.2.3.1. Verification

For verification of the reduced-order model, especially the aerodynamics and the coupling process, two basic aeroelastic phenomena are considered, i.e. static divergence and bending torsion flutter.

For static divergence, a simple torsion bar is examined, which is estimated to deform in the shape of the first torsional mode of the structure. The aerodynamics are modelled according to potential flow around a flat plate. This model results in a divergence speed of 915 m/s. The reduced-order model gives a value of 927 m/s, which is almost the same, although the presented aerodynamic model is invalid at this speed, of course.

Considering bending torsion flutter, the unsteady aerodynamic model used by Haas and Chopra in [18] is implemented, which is based on Theodorsen's theory [20]. This results in a flutter speed of 347 m/s, whereas the model based on unsteady flow simulations yields a flutter speed of 364 m/s. Again, the results are comparable.

4.2.3.2. Circulation Control Flutter

Haas and Chopra [18] also found a phenomenon which they termed "circulation control flutter". It is a single degree of freedom bending flutter, which occurs at high blowing rates and small angles of attack. To demonstrate this, a configuration is chosen with a flap deflection of 65° and an angle of attack of the aircraft of 3°. FIGURE 12 shows the resulting oscillation of the first two bending modes for blowing coefficients of 0.03 and 0.05.

The first case shows a damped oscillation, whereas in the second case, it is excited only due to the increased blowing. A solution in the frequency domain gives the same effect. For a linearized equation of motion, a modal analysis gives the eigenvalues of the system

(5) $\lambda = \delta \pm i\omega$,

where δ is a measure for the damping of the corresponding mode.

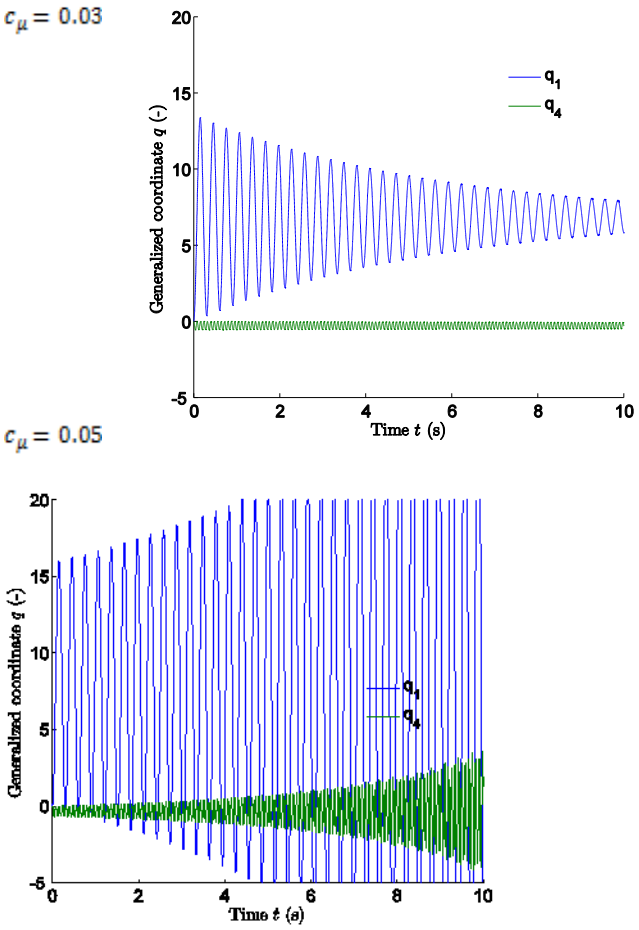

FIGURE 12: Bending Oszillations

FIGURE 13 shows the damping of the first six natural modes dependent on the velocity of approach for blowing coefficients of 0.04 and 0.05.

Again, in the first case the system is stable. With increased blowing, the first mode, which refers to bending, becomes unstable for any velocity. Omitting all modes except the first basically yields the same results.

4.2.3.3. Connection to flight dynamics model

The presented model for the elastic wing may be connected as an additional module to the flight dynamics model of flight control project. The existing model hands the current state of the rigid body aircraft over to the elastic wing module. The current state is represented by the true air speed, the dynamic pressure, the angle of attack of the rigid body aircraft, as well as global values for the flap deflection angle and the blowing coefficient. The elastic wing module returns the variation of the aerodynamic loads due to the deformation of the wing.

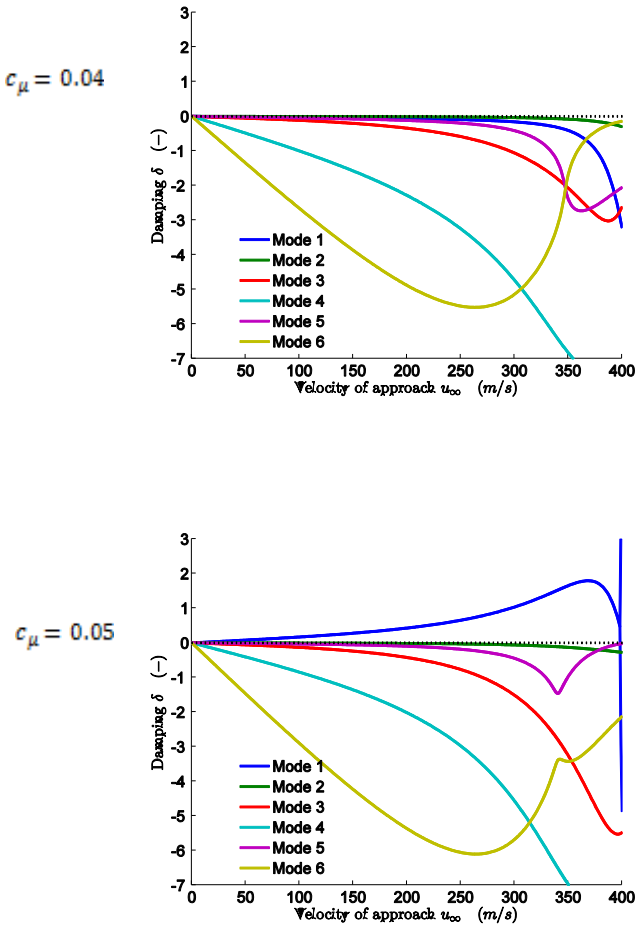

FIGURE 13: Damping and blowing rate

The equation of motion of the rigid body aircraft may be written as

$$(6)\quad \mathbf{M}\,\ddot{\mathbf{x}} = \mathbf{L}_{\text{rigid}} + \Delta\mathbf{L}_{\text{elastic}}(\mathbf{q}, \dot{\mathbf{q}}, \ddot{\mathbf{q}}) \,,$$

where $\mathbf{L}_{\text{rigid}}$ contains all the loads from the rigid body model, which are not considered in detail here. The variation of the aerodynamic loads depends on the current state of the elastic wing, which results from the equation of motion

$$(7)\quad \ddot{q} + \omega_i^2\, q_i = f_{Ai}(\mathbf{x}, \dot{\mathbf{x}}, \ddot{\mathbf{x}}) \,,$$

where the right-hand side depends on the current state of the rigid body aircraft, again, so that the system is coupled in both directions.

5. ACKNOWLEDGEMENT

The authors thankfully acknowledge the funding of the work by the German Science Foundation (DFG) in the frame of the Coordinated Research Centre SFB880.

6. LITERATURE

[1] Radespiel, R., Heinze, W., SFB880 - Fundamentals of High Lift for Future Commercial Aircraft. Proceedings Deutscher Luft- und Raumfahrtkongress, 10.-12. September 2013, Stuttgart, Germany, 2013

[2] Keller, D., Numerical Approach Aspects for the Investigation of the Longitudinal Static Stability of a Transport Aircraft with Circulation Control. Notes on Numerical Fluid Mechanics and Multidisciplinary Design. to be published.

[3] Keller, D., Rudnik, R., Aerodynamic Aspects of the Longitudinal Motion of a High-Lift Aircraft Configuration with Circulation Control. *SFB 880 - Fundamentals of high-lift for future commercial aircraft, Biennial report.* s.l. : Shaker Verlag, 2013.

[4] Keller, D., *Numerical Investigation of Engine Effects on the Stability and Controllability of a Transport Aircraft with Circulation Control.* s.l. : AIAA, 2013. 2013-3031.

[5] Werner-Westphal, Christian, Wolfgang Heinze, and Peter Horst: Multidisciplinary Integrated Preliminary Design Applied to Future Green Aircraft Configurations. In Aerospace Sciences Meetings, American Institute of Aeronautics and Astronautics, Reno, NV, USA, January 2007.

[6] Keller, D.: Numerical Investigation of the Longitudinal Static Stability of a Transport Aircraft with Circulation Control. In Proceedings of the 18th DGLR-STAB Symposium, Stuttgart, Germany, 2012.

[7] Raab, C.: A Versatile and Modular Architecture for Aircraft System Simulation and Test. Institute report IB 111-2006/22, Institute of Flight Systems, DLR, Braunschweig, Germany, 2006.

[8] Radespiel, R, K Pfingsten, and C Jensch: Flow Analysis of Augmented High-Lift Systems. Hermann Schlichting – 100 Years, Notes on Numerical Fluid Mechanics and Multidisciplinary Design, 102:168-189, 2009.

[9] Pfingsten, K C and R Radespiel: Numerical simulation of a wing with a gapless high lift system using circulation control. New Results in Numerical and Experimental Fluid Mechanics, VI:71–79, 2008.

[10] Gerhold, T.: Overview of the Hybrid RANS Code TAU. In Kroll, N. and J. Fassbender (editors): MEGAFLOW – Numerical Flow Simulation for Aircraft Design, volume 89 of Notes on Numerical Fluid Mechanics and Multidisciplinary Design, pages 81–92. Springer Verlag, Berlin Heidelberg, Germany, 2005.

[11] Brockhaus, R., W. Alles, and R. Luckner: Flugregelung. Springer Verlag, Berlin, Heidelberg, Germany, 2010.

[12] Mönnich, W.: Ein 2-Punkt-Aerodynamikmodell für die Identifizierung. In Proceedings of Systemidentifikation in der Fahrzeugdynamik: Symposium des Sonderforschungsbereichs 212: Sicherheit im Luftverkehr, DFVLR-Mitteilungen 87-22, Braunschweig, Germany, 1987.

[13] Diekmann, J.H.: Nonlinear Flight Dynamics Simulation Model for a Civil Aircraft with Active High Lift System, Institute report IB 111-2013/15, Institute of Flight Systems, DLR, Braunschweig, Germany, 2013.

[14] Jensch, K., Pfingsten, K. C., Radespiel, R., Schuermann, M., Haupt M. and Bauss S., Design aspects of a gapless High-Lift system with active blowing, Deutscher Luft- und Raumfahrtkongress, (2009), pp. 1-7.

[15] Haupt, M., Niesner, R., Unger, R., and Horst, P., Computational aero-structural coupling for hypersonic applications, AIAA 2006-3252, 9th AIAA/ASME Joint Thermophysics and Heat Transfer Conference, 2006

[16] Sommerwerk, K. and Haupt, M., Structural Sizing of a CFRP Wing with Coandă Flaps via CFD-CSM Coupling, Deutscher Luft- und Raumfahrtkongress, 2012, pp. 1–10
[17] Sommerwerk, K., Haupt, M. and Horst P., Aeroelastic Performance Assessment of a Wing with Coandă Effect Circulation Control via Fluid-Structure Interaction, AIAA-2013-2791, 31st AIAA Applied Aerodynamics Conference; June 24-27, 2013, San Diego, pp. 1-13
[18] Haas, D. and I. Chopra. Flutter of circulation control wings. *Journal of Aircraft*, 26(4):373–381, 1989.
[19] Schwamborn, D., A. Gardner, H. von Geyr, A. Krumbein, H. Lüdeke and A. Stürmer. Development of the TAU-Code for aerospace applications. *50th NAL International Conference on Aerospace Science and Technology*, Bangalore (India), 2008.
[20] Theodorsen, T., General theory of aerodynamic instability and the mechanism of flutter. *NACA report No. 496*, 1935.